

Mechanism of Protein Aggregation Inhibition by Arginine: Blockage of Anionic Side Chains Favors Unproductive Encounter Complexes

Yuen Ki Ng and Lars Konermann*



Cite This: *J. Am. Chem. Soc.* 2024, 146, 8394–8406



Read Online

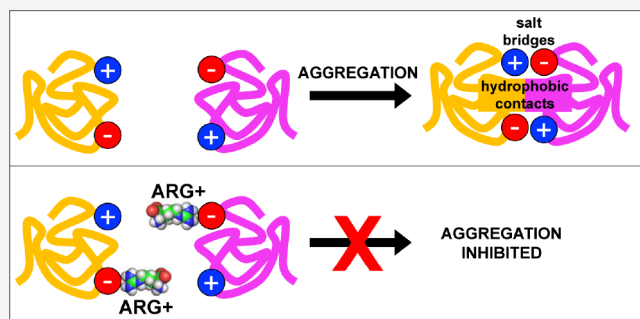
ACCESS |

Metrics & More

Article Recommendations

Supporting Information

ABSTRACT: Aggregation refers to the assembly of proteins into nonphysiological higher order structures. While amyloid has been studied extensively, much less is known about amorphous aggregation, a process that interferes with protein expression and storage. Free arginine (Arg^+) is a widely used aggregation inhibitor, but its mechanism remains elusive. Focusing on myoglobin (Mb), we recently applied atomistic molecular dynamics (MD) simulations for gaining detailed insights into amorphous aggregation (Ng et al. *J. Phys. Chem. B* 2021, 125, 13099). Building on that approach, the current work for the first time demonstrates that MD simulations can directly elucidate aggregation inhibition mechanisms. Comparative simulations with and without Arg^+ reproduced the experimental finding that Arg^+ significantly decreased the Mb aggregation propensity. Our data reveal that, without Arg^+ , protein–protein encounter complexes readily form salt bridges and hydrophobic contacts, culminating in firmly linked dimeric aggregation nuclei. Arg^+ promotes the dissociation of encounter complexes. These “unproductive” encounter complexes are favored because Arg^+ binding to D^- and E^- lowers the tendency of these anionic residues to form interprotein salt bridges. Side chain blockage is mediated largely by the guanidinium group of Arg^+ , which binds carboxylates through H-bond-reinforced ionic contacts. Our MD data revealed Arg^+ self-association into a dynamic quasi-infinite network, but we found no evidence that this self-association is important for protein aggregation inhibition. Instead, aggregation inhibition by Arg^+ is similar to that mediated by free guanidinium ions. The computational strategy used here should be suitable for the rational design of aggregation inhibitors with enhanced potency.



INTRODUCTION

The folded structures of native proteins are stabilized by a network of noncovalent contacts.¹ Unfortunately, proteins can also aggregate, i.e., assemble into nonphysiological complexes. Such aggregates range from small soluble oligomers to macroscopic precipitates.^{2–7} Aggregation is an active area of research.^{3,8–11} Most work in this field has focused on amyloid and amyloid precursors, i.e., highly ordered aggregates that are associated with various diseases.^{3,9,10,12–14} Other aggregates are disordered (amorphous),^{15,16} as often seen in aged solutions or after exposure to unfavorable conditions such as elevated temperature.^{17–23} Amorphous aggregates give protein samples a milky appearance that arises from Rayleigh scattering of precipitated particles.²⁴ Amorphous aggregation lowers the yield of recombinant proteins,^{25–27} limits the shelf life of biopharmaceuticals,^{7,28–30} and can trigger adverse immune responses.³¹

The many detrimental aspects of protein aggregation have sparked interest in strategies that inhibit aggregation.^{32,33} Molecular chaperones are proteins that sequester aggregation-prone chains and promote their proper folding.^{10,34–39} Chemical chaperones are natural or synthetic aggregation inhibitors^{40–43} ranging from nanoparticles^{42,44} to low MW

additives such as amino acids, sugars, surfactants, alcohols, salts, and nucleoside triphosphates.^{26,30,42,45–47} Mixtures of these compounds serve as excipients in biopharmaceutical formulations, where they promote protein longevity.⁴⁸ The optimization of such formulations requires time-consuming trial-and-error assays.^{49–51} A better understanding of aggregation inhibition would help streamline the excipient screening process.⁵²

Free arginine (Arg^+) is one of the most common chemical chaperones.^{27,41,53–56} The net positive charge of this amino acid at pH 7 arises from its $[-\text{HN}-\text{C}(\text{NH}_2)_2]^+$ guanidinium (Gdn^+) group that is connected to the zwitterionic ${}^+\text{H}_3\text{N}-\text{C}_\alpha\text{H}-\text{COO}^-$ moiety by a propyl linker.⁵⁷ Commercially available Arg^+Cl^- is denoted as Arg-HCl. Following the discovery of Arg^+ -mediated aggregation inhibition in the

Received: December 14, 2023

Revised: January 31, 2024

Accepted: February 22, 2024

Published: March 13, 2024



1990s,⁵⁸ up to 1 M Arg-HCl is now routinely used for biotechnological applications.^{25,59} Efforts are underway to develop Arg⁺-derived compounds that are even more potent aggregation inhibitors for *in vitro* and *in vivo* applications.^{53,55}

The mechanism whereby Arg-HCl inhibits protein aggregation remains controversial.^{55,60–62} One proposal envisions the formation of Arg⁺ clusters with extensive hydrophobic surfaces that sequester nonpolar sites of aggregation-prone proteins.⁶³ Self-association of Arg⁺ has been confirmed by molecular dynamics (MD) simulations, but those simulations refuted the idea that Arg⁺ clustering generates hydrophobic surfaces.⁶⁰ Instead, it was proposed that Arg⁺-clusters suppress aggregation nuclei by “neutral crowding”.^{60,64,65} Other work suggested that aggregation inhibition involves Arg⁺ binding to various side chains including D[−], E[−], W, H, and others.^{54,59,61,66} Binding of Arg⁺ to these residues may resemble interactions taking place between proteins and free Gdn⁺ ions. However, the prevailing view is that Gdn⁺ and Arg⁺ act very differently, with Arg-HCl being an aggregation inhibitor that “stabilizes” native proteins, while Gdn-HCl is a denaturant.^{61,62,67,68} Overall, a compelling explanation why Arg-HCl inhibits aggregation is still missing.

Similar to Arg⁺, lysine (Lys⁺) has a positively charged side chain. Lys⁺ can also suppress protein aggregation to some extent.⁶⁹ However, the efficacy of Lys⁺ is lower than that of Arg⁺, making Arg⁺ a much more widely used aggregation inhibitor.^{25,54,55,58–66} For this reason, the focus of the current work is on the mechanism of Arg⁺-induced aggregation inhibition.

MD simulations have become an essential tool for probing protein folding and dynamics.^{70–73} In contrast, MD investigations of aggregation are rare and limited largely to amyloid.^{9,74–76} Only a handful of MD studies have tackled questions related to aggregation inhibition.⁷⁷ Some of those simulations explored inhibitor binding to monomeric proteins,^{60,78–80} peptides,⁴⁷ or peptide oligomers.⁵⁴ However, none of those studies have modeled actual aggregation events, thereby precluding direct insights into inhibition mechanisms.

We recently demonstrated that atomistic MD simulations in explicit water are suitable for modeling amorphous aggregation, using myoglobin (Mb) as a test system.⁸¹ Mb is a paradigmatic globular protein that has previously served to uncover fundamentals of folding,⁸² thermodynamics,⁸³ conformational fluctuations,⁸⁴ and amyloid formation.⁸⁵ The Mb propensity to form amorphous aggregates upon heating is well known.^{24,86} The lack of Cys in Mb eliminates complications related to non-native disulfide bonding.^{87,88} Our earlier data⁸¹ revealed that the sequential assembly of thermally unfolded Mb monomers into oligomeric aggregates primarily involves hydrophobic contacts and salt bridges.

The current work uncovers the mechanism whereby Arg⁺ inhibits thermal protein aggregation. After conducting a number of experiments, we performed extensive MD simulations to elucidate atomistic details of Mb aggregation in the presence and absence of Arg⁺. These simulations reproduced the experimental finding that Arg⁺ greatly reduces the protein aggregation propensity. The root cause of aggregation inhibition was found to be binding of Arg⁺ to anionic side chains via H-bond-reinforced ionic contacts. Blocking these side chains interferes with the formation of interprotein salt bridges, causing protein–protein encounter complexes to dissociate instead of forming firmly linked aggregates. These Arg⁺-mediated events are analogous to

aggregation inhibition by free Gdn⁺ ions, which were examined here as well. It appears that this work marks the first time that MD simulations directly captured the occurrence of protein aggregation inhibition, allowing the underlying mechanism to be uncovered by inspection of atomistic trajectories.

METHODS

Thermal Aggregation Experiments. Horse-heart ferri-Mb, L-Arg-HCl, Gdn-HCl, and Gly were obtained from Sigma (St. Louis, MO). NaCl, and monobasic/dibasic sodium phosphate were from Caledon (Georgetown, ON). All Mb samples contained 50 mM sodium phosphate and 100 mM NaCl in water at pH 7; this solvent will be referred to as “buffer”. Mb stock solutions were centrifuged to remove small amounts of insoluble debris. Thermal aggregation was probed by immersing Eppendorf tubes containing 100 μL of 100 μM Mb (in buffer without and with various additives) in a water bath for 10 min at temperatures (*T*) between 20 and 95 °C. The samples were then centrifuged for 2 min at 15,000 g at 4 °C for pelleting aggregated precipitate. To quantify the leftover soluble Mb, the supernatant was analyzed at room temperature (22 ± 1 °C) using a Bioteck Epoch 2 spectrophotometer (Agilent, Mississauga, ON) with a Take3 microvolume plate by measuring the absorbance (*A*) at 409 and 280 nm. The data were processed as (% soluble protein remaining) = 100% × *A*(*T*)/*A*(20 °C).

Unfolding Experiments. For studying thermal unfolding in the absence of aggregation, the Mb concentration was lowered to 5 μM, taking advantage of the fact that aggregation is strongly concentration dependent.⁸¹ Unfolding profiles were acquired between 20 and 95 °C by circular dichroism (CD) spectroscopy, using a Jasco J-810 instrument (Easton, MD) with a 1 mm cuvette to monitor the ellipticity at 222 nm (CD₂₂₂). In addition, unfolding profiles were generated by monitoring the absorbance at 409 nm on a Cary 3500 multicell spectrophotometer (Agilent, Santa Clara, CA). To facilitate a side-by-side comparison with the CD₂₂₂ data, A₄₀₉ profiles were normalized using

$$\text{Normalized Absorbance} = \frac{A(T) - A(20^\circ \text{ C})}{A(95^\circ \text{ C}) - A(20^\circ \text{ C})} \quad (1)$$

Spectroscopically detected thermal unfolding profiles were fitted using^{57,89}

$$X(T) = \frac{(y_N + m_NT) + (y_U + m_UT)\exp\left(-\frac{\Delta G(T)}{RT}\right)}{1 + \exp\left(-\frac{\Delta G(T)}{RT}\right)} \quad (2)$$

where X(*T*) denotes the CD₂₂₂(*T*) or the normalized A₄₀₉(*T*) profiles. The free energy of unfolding in eq 2 is $\Delta G(T) = \Delta H(1 - T/T_m)$, where *T_m* denotes the melting temperature, while (y_N + m_N*T*) and (y_U + m_U*T*) are the pre- and post-transition baselines. The enthalpy of unfolding (ΔH) was assumed to be constant.⁸⁹ Fitted parameters and their standard deviations were determined from at least three independent replicate scans at 4 K min^{−1} or 1 K min^{−1}; no differences were observed for these two scan rates, and the latter was used for most measurements. Blanks were subtracted for the UV-vis data.

Molecular Dynamics. MD simulations were conducted following a strategy similar to that described previously.⁸¹ Briefly, GROMACS 2018.3⁷³ was used with the CHARMM36m force field⁹⁰ and TIP3P water.⁹¹ The CHARMM/TIP3P combination has been remarkably successful for modeling protein folding and dynamics.⁷⁰ The 36m version of this force field was optimized for studies on non-native structures that are the focus of the current work.⁹⁰ Also, the CHARMM parametrization of Arg⁺ used here has been shown to be well suited for capturing protein-Arg⁺ interactions.^{60,92} Trajectories were generated using the leapfrog algorithm with a 2 fs time step. Gdn⁺ parameters were taken from CHARMM-GUI.⁹³ Periodic boundary conditions (PBCs) were applied with a minimum distance of 1 nm between the protein atoms and PBC box boundaries. The cubic PBC box was lined with a layer of partially immobilized water to

prevent artifacts arising from protein diffusion across box boundaries.⁸¹ We previously validated this approach for aggregation simulations, verifying the absence of spurious protein interactions with PBC walls.⁸¹ Nonbonded interactions used a 1.2 nm cutoff. Long-range electrostatics were treated using particle-mesh Ewald summation. Following steepest descent energy minimization, all runs employed 100 ps of *NVT* and 100 ps of *NPT* equilibration, prior to *NPT* production runs. In accordance with experimental conditions, the temperature and pressure were kept at 370 K and 1 bar, respectively. Protein charges were set to their pH 7 values, i.e., Nt⁺ (N-terminus), R⁺, K⁺, H⁰, D⁻, E⁻, and Ct⁻ (C-terminus).⁵⁷ To match the 150 mM ionic strength used in our experiments, 150 mM Na⁺ and Cl⁻ were randomly inserted (for simplicity, we will refer to these conditions as “water”). Free Arg⁺ was modeled with a zwitterionic $^+H_3N-C_aH-COO^-$ headgroup and a positive Gdn side chain.⁶⁰ Arg⁺ or free Gdn⁺ were balanced by additional Cl⁻ to ensure charge neutrality.

Thermally unfolded monomeric apo-Mb starting structures were generated from electrostatically stretched initial conformers. These structures were then relaxed for 50 ns at 370 K.⁸¹ This relaxation was performed under three conditions: in water, in 1 M Arg-HCl, and in 1 M Gdn-HCl (for details, see Figure S1). Starting structures for aggregation simulations were selected randomly from the 35 to 50 ns interval at the desired solvent composition.

Aggregation was simulated by positioning two unfolded Mb chains in random orientations with randomly chosen conformations in a $(17 \pm 3 \text{ nm})^3$ PBC box. Initial placements where the two chains were already in van der Waals contact were discarded. To examine the effects of solution conditions (water, 1 M Arg-HCl, or 1 M Gdn-HCl), runs were performed in triplicate sets. Each set employed identical run times, PBC box sizes, and initial protein coordinates, with the latter being obtained from equilibration runs in water (blue in Figure S1D). To speed up the simulations, some runs were transferred to a smaller PBC box once the proteins had aggregated. To maintain comparability, these box size changes were simultaneously applied to all runs within each triplicate set. Final box sizes were $(16 \pm 3 \text{ nm})^3$. A triplicate set of simulations was terminated once one of the runs had firmly aggregated, often for >100 ns (but no less than 20 ns). “Aggregated” in this context means that the two chains maintained a minimum distance of less than 0.25 nm, reflecting intermolecular van der Waals contacts (usually between hydrophobic residues) and/or H-bonding (typically in combination with salt bridge formation). Similarly, doublet sets of simulations were performed to further compare aggregation in water vs 1 M Arg-HCl, using starting structures that had been equilibrated in 1 M Arg-HCl (black in Figure S1D). Additional doublet sets were performed in water vs 1 M Gdn-HCl, using starting structures equilibrated in 1 M Gdn-HCl (red in Figure S1D), for a total of 56 aggregation simulations. The total simulation time of all runs was $\sim 12 \mu\text{s}$, with an average of $\sim 500,000$ atoms per run.

RESULTS AND DISCUSSION

Aggregation Inhibition by Arg-HCl and its Building Blocks. We started our investigation into the mechanism of Arg-HCl aggregation inhibition by conducting experiments to provide a foundation for subsequent MD simulations. Heating to 95 °C of 100 μM Mb in buffer without additives gave the initially clear samples a cloudy appearance, representing the hallmark of amorphous aggregation.^{17–24} The aggregates formed distinct pellets after centrifugation (Figure 1A). Strikingly, in 1 M Arg-HCl most of the Mb remained in solution (Figure 1B), as seen from the red-brown (heme) color of the supernatant and the much smaller pellet. This test confirms the remarkable capability of Arg-HCl to suppress protein aggregation.^{25,27,41,53–56,58,59,94,95}

Can aggregation inhibition be attributed to a specific moiety of Arg-HCl? We attempted to identify this “active component” by dissecting Arg-HCl into its building blocks.^{41,62,96} These

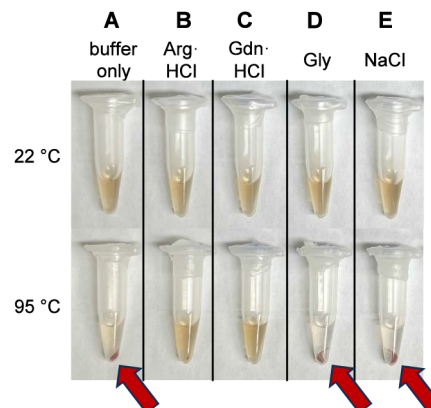


Figure 1. Photographs of 100 μM Mb in buffer (A) without additive and in the presence of 1 M (B) Arg-HCl, (C) Gdn-HCl, (D) Gly, and (E) NaCl at 22 °C (top row). The bottom row shows the samples after 10 min at 95 °C followed by centrifugation. Arrows in panels A, D, E point to centrifugation pellets consisting of aggregated Mb.

building blocks are Gdn⁺, propane, and Gly (see the structures in Figure 2). In addition, the increased Cl⁻ content or ionic strength of 1 M Arg-HCl could play a role. Experiments on heated solutions containing 1 M propane are not feasible, but testing the remaining three components is straightforward. Thus, we examined Mb solutions containing 1 M of either Gdn-HCl, Gly, or NaCl. The latter was included to examine the effects of Cl⁻ and ionic strength. Similar to Arg-HCl, Gdn-HCl was highly effective at inhibiting aggregation (Figure 1C). No inhibitory effect was found for Gly or NaCl (Figure 1D,E).

The observation that neither the $^+H_3N-C_aH-COO^-$ moiety nor increased ionic strength is responsible for aggregation inhibition suggests that the active component of Arg-HCl is its Gdn⁺ group. This proposal may seem tenuous when considering only the data in Figure 1. However, the following sections present several lines of evidence to support the idea that aggregation inhibition by Arg-HCl and Gdn-HCl can be attributed to basically the same Gdn⁺-mediated mechanism.

Quantitative Aggregation Assays. UV-vis assays were conducted at various temperatures to characterize Mb aggregation in more detail (see Methods). Two wavelengths were monitored to avoid pitfalls that might potentially be associated with the simple tests of Figure 1: A_{409} probes the heme Soret band,⁹⁷ while A_{280} reports on Trp absorbance with minor contributions from other aromatic side chains.⁹⁸ Soret measurements may underestimate the concentration of soluble Mb if heme (which is insoluble at pH 7) dissociates from the protein.⁸² Conversely, A_{280} may overestimate the concentration if there is residual background scattering.²⁴ Thus, the actual concentration of nonaggregated protein after heating will be between the values determined from A_{409} and A_{280} .

Heating without additives triggered a sharp decrease in A_{409} and A_{280} between 75 and 80 °C, marking the onset of Mb aggregation in this temperature range (Figure 2A).^{24,86} Only 19% of soluble Mb remained at 95 °C, as determined from the averaged A_{409} and A_{280} readings. UV-vis profiles for Arg-HCl showed a slight dip around 70 °C, but the soluble Mb fraction increased again upon raising the temperature further. At 95 °C, the fraction of soluble Mb was 78% (Figure 2B). These data reaffirm the capability of Arg-HCl to inhibit aggregation. The slight dip around 70 °C suggests that the Arg-HCl effects are

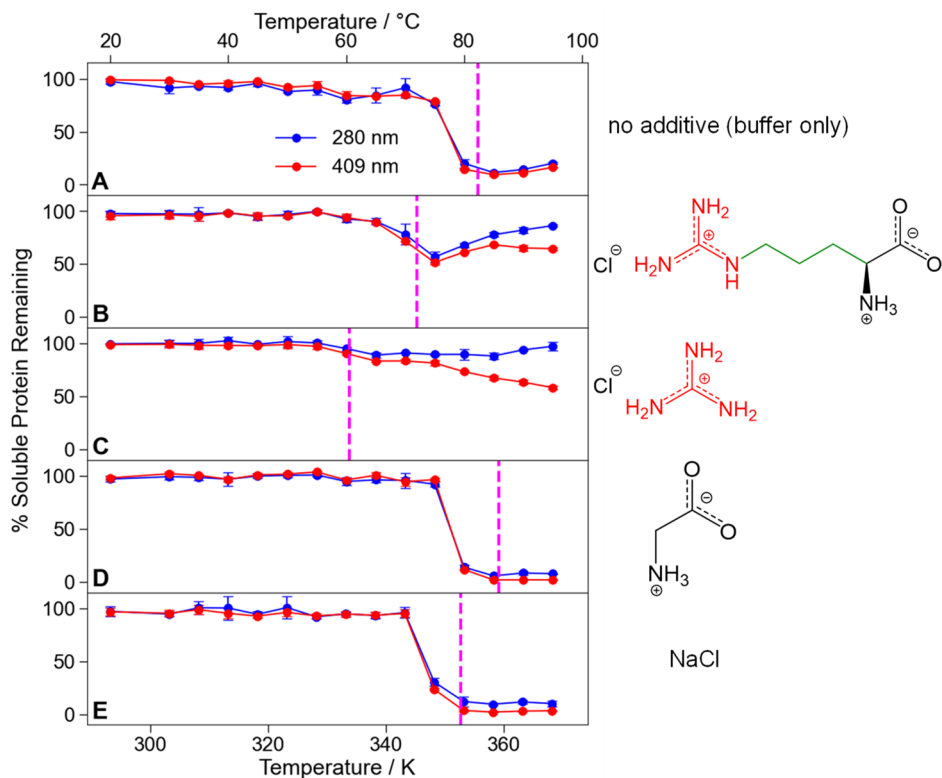


Figure 2. UV-vis Mb aggregation assays probed at 409 and 280 nm, after 10 min of heating to the specified temperature with different 1 M additives. (A) Buffer without additives. (B) With Arg-HCl. (C) With Gdn-HCl. (D) With Gly. (E) With NaCl. Each data point represents the average of triplicate measurements. Error bars represent standard deviations. Vertical dashed lines indicate T_m values, measured at a lowered Mb concentration where aggregation is negligible (Figure S2).

somewhat temperature dependent, with aggregation suppression being more effective at 95 °C than at 70 °C.

The fraction of soluble protein in Gdn·HCl at 95 °C was 79% (Figure 2C), similar to that in Arg-HCl at 95 °C. UV-vis profiles for Gly and NaCl (Figure 2D,E) resembled the “no additive” results of Figure 2A. These quantitative aggregation data mirror the trends seen in Figure 1, consistent with the proposal that the Gdn⁺ group of Arg-HCl is mainly responsible for aggregation inhibition.

The assays in Figures 1 and 2 employed a heat incubation period of 10 min. Time-dependent data revealed that extended (24 h) exposure to 95 °C caused complete aggregation, even in the presence of Arg-HCl or Gdn-HCl (Figure S3). Thus, both Arg-HCl and Gdn-HCl act by lowering the aggregation rate, rather than changing the equilibrium between soluble and aggregated Mb.

While the high temperatures explored in our experiments do not have direct physiological relevance, this range is typical for unfolding experiments aimed at uncovering protein thermodynamic parameters.^{83,89} More importantly, the use of such high temperatures is common for accelerated screening assays that assess the structural resilience and the shelf life of monoclonal antibodies and other protein therapeutics.^{49,50,99,100}

Effects of Additives on Native State Stability. Globular proteins become susceptible to aggregation after partial or global unfolding.^{3,101–106} Previous work has established that Mb thermal aggregation follows a *Native* → *Globally Unfolded* → *Aggregated* sequence.^{81,86} For this two-step sequence, aggregation inhibitors may act by two approaches: (i) Stabilization of the native state against unfolding will disfavor the first step. (ii) Interfering with protein–protein contacts

among unfolded chains will disfavor the second step.⁴⁵ Measurements of the native state stability offer a way to distinguish between these two options. Specifically, scenario (i) should be associated with a T_m shift to higher temperature.⁸³

CD and UV-vis unfolding assays were performed at a lowered Mb concentration of 5 μM, where aggregation is negligible⁸¹ (Figure S2). T_m values measured in these assays are included in Figure 2 as vertical dashed lines. Interestingly, Arg-HCl destabilizes the native state, evident from a T_m shift from 82 to 72 °C. An even more pronounced destabilization was observed for Gdn·HCl, with T_m = 61 °C. In contrast, Gly slightly stabilized the native state (T_m = 86 °C), while the behavior with NaCl (T_m = 80 °C) was similar to that without additive. These T_m trends are consistent with earlier work on Mb and other proteins.^{62,81} The results imply that neither Arg-HCl nor Gdn-HCl inhibits aggregation by stabilizing the native state against unfolding. Instead, we conclude that both interfere with the formation of protein–protein contacts among unfolded chains, consistent with scenario (ii). From the MD data discussed later in this work, it can be seen that this inhibition of protein–protein contacts is the result of suppressed salt bridge formation.

Native State Destabilization by Arg-HCl. The observation that Gdn-HCl renders Mb more susceptible to thermal unfolding (Figures 2 and S2) is trivial, because this additive is a widely used denaturant.⁵⁷ Native state destabilization by Arg-HCl is more surprising, considering that earlier studies distinguished between the *denaturant* Gdn-HCl and the *protein stabilizer* Arg-HCl.^{57,62,67,107} However, the data of Figure 2, along with earlier work,^{62,108} suggest that such a distinction is misleading. This is because both Gdn-HCl and Arg-HCl inhibit

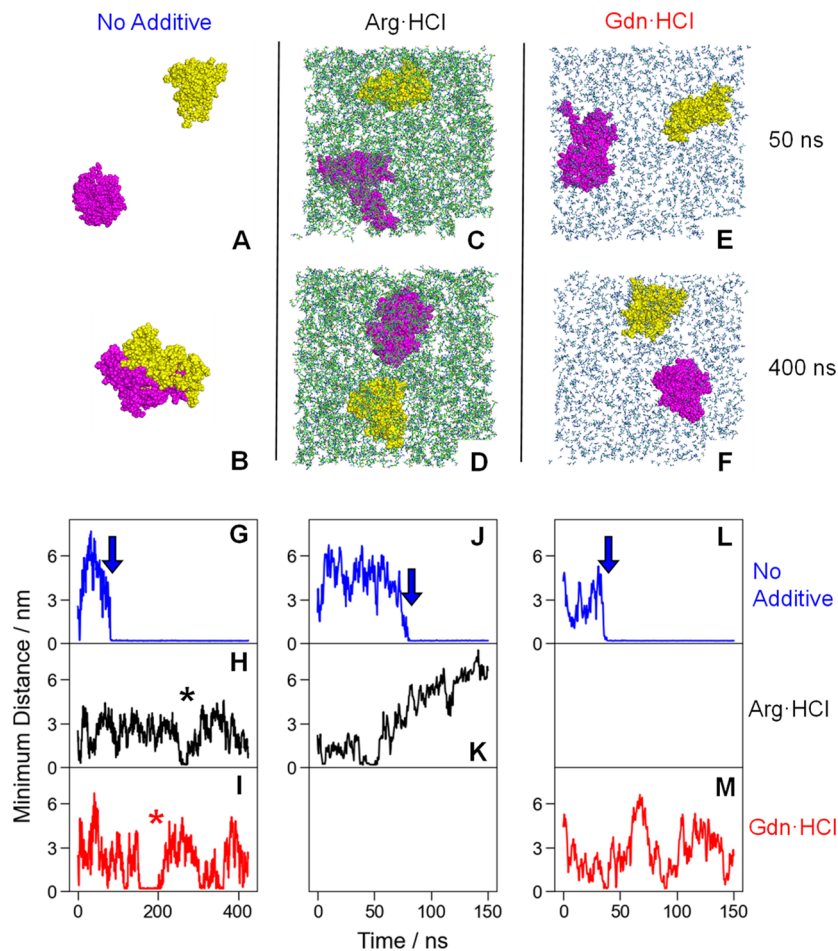


Figure 3. Representative MD data for the aggregation of two Mb chains (yellow and magenta). Top panels: snapshots for $t = 50$ and 400 ns; (A,B) without additive; (C,D) in 1 M Arg·HCl; (E,F) in 1 M Gdn·HCl. See also [SI movie](#). Additives in panels C–F are shown in green or gray; water, Na^+ , and Cl^- have been omitted for visualization. Bottom panels: time profiles of minimum chain distance for initial structures equilibrated (G–I) in water, (J,K) in 1 M Arg·HCl, and (L,M) in 1 M Gdn·HCl. Arrows in panels G–L indicate formation of productive encounter complexes (PECs) leading to irreversible aggregation. Panel H and I asterisks represent unproductive encounter complexes (UECs) that dissociate again. Data in A–F were taken from panel G–I trajectories.

aggregation and both destabilize the native state during thermal unfolding (as well as chemical unfolding, [Figure S4](#)). These findings demonstrate that the effects of Arg·HCl and Gdn·HCl are quite similar.

We posit that the widespread habit of referring to Arg·HCl as a “protein stabilizer” is based on imprecise usage of this term.^{57,62,67,107,108} Consistent with previous work,⁶² our data show that Arg·HCl shifts the $\text{N} \rightleftharpoons \text{U}$ equilibrium to the right. By definition, therefore, Arg·HCl causes thermodynamic destabilization of the native state.^{1,57,108} The ability of Arg·HCl to suppress aggregation by keeping proteins soluble should not be confused with thermodynamic stabilization.^{1,57,108} The reason why Arg·HCl is not categorized as a denaturant lies in its relatively low solubility (~ 1 M), while the higher solubility of Gdn·HCl (~ 7 M) facilitates the preparation of solutions that trigger unfolding.⁵⁷

Is the native state destabilization by Arg·HCl seen here and elsewhere⁶² consistent with its use as an excipient in biopharmaceutical formulations?^{26,30,42,45,48} It would be counterproductive to employ an excipient that suppresses aggregation while causing unfolding (and thus protein deactivation). Luckily, destabilization of the native state by 1

M Arg·HCl (or 1 M Gdn·HCl) is insufficient for causing room temperature unfolding of Mb ([Figure S4](#)) and other proteins.⁶²

Overview of MD Simulation Results. MD simulations were conducted to provide an atomistic underpinning of the experiments discussed above. Our simulations compared the Mb aggregation propensity without additive, with 1 M Arg·HCl, and with 1 M Gdn·HCl. Aggregates formed under the conditions of [Figure 1](#) comprise trillions of proteins. Tackling such large systems in atomistic MD runs is not feasible. To keep the computational cost manageable, we focused our simulations on the formation of dimeric aggregates from monomeric chains. Such dimeric nuclei represent the initial step of any aggregation process.^{109,110} Also, it has been noted that key aspects of aggregation (and aggregation inhibition) should already manifest themselves during this monomer \rightarrow dimer transition.⁶⁰ MD runs were conducted at 370 K, because [Figure 2](#) revealed that aggregation is most prevalent in this range; 370 K is well above T_m ([Figure S2](#)). Therefore, all MD runs started from unfolded Mb. The two chains were fully separated at the onset of each run.

Typical simulation snapshots are depicted in [Figure 3A–F](#). For the runs highlighted in these panels, all of the chains remained separated after 50 ns. By 400 ns, the “no additive”

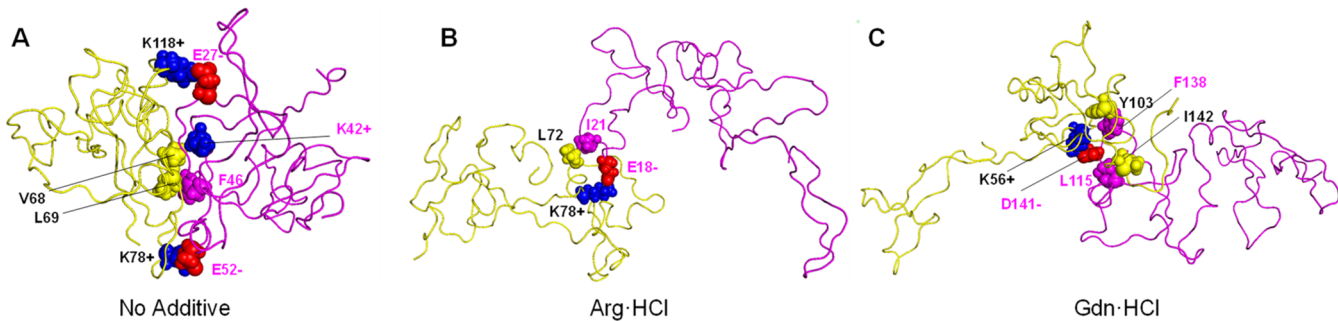


Figure 4. Representative protein–protein contacts in mature dimeric aggregates, representing simulation end points under different conditions. (A) No additive, (B) with Arg·HCl, and (C) with Gdn·HCl. The two chains are depicted in yellow and magenta. Residues involved in intermolecular contacts are shown in spacefill representation. Hydrophobic residues (L, I, V, F, W) are yellow and magenta; positively charged residues (K^+ , R^+) are blue; negatively charged residues (D^- , E^-) are red. Contact residues were identified by comparing solvent-accessible surface areas in aggregates relative to those of monomeric substructures.⁸¹

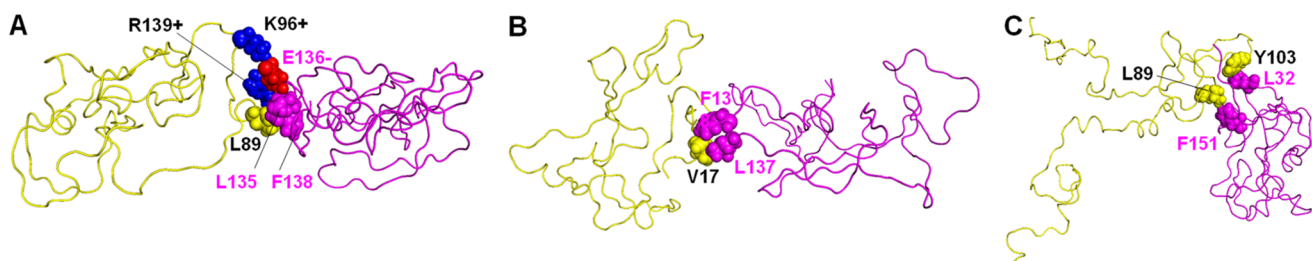


Figure 5. Representative examples of productive encounter complexes (PECs) formed (A) without additive, (B) with Arg·HCl, and (C) with Gdn·HCl. Coloring and notation are identical with those in Figure 4. Note that PEC formation in Arg·HCl and Gdn·HCl is rare, and that the PECs in panels B and C do not possess (blue/red) intermolecular salt bridges.

run had produced a dimeric aggregate (Figure 3B), while the chains in Arg·HCl and Gdn·HCl did not associate (Figure 3D,F). For probing protein–protein interactions in more detail, we tracked the minimum interchain distance vs time. Prior to aggregation, distance values fluctuated widely, reflecting the independent diffusive motions of the two chains. Aggregation was marked by a striking drop down to ~ 0.25 nm ($t = 83$ ns, see arrow in Figure 3G), indicating that atoms from both chains were in van der Waals and/or H-bonding contact with one another. For the Arg·HCl and Gdn·HCl runs, there was no aggregation during the 425 ns window, despite some brief encounters (asterisks in Figure 3H,I).

Figure 3G–I represents a triplicate set of simulations that share identical PBC box sizes, run times, and initial protein coordinates. The latter had been equilibrated in water. It might be argued that this equilibration is not suitable for simulations in Arg·HCl or Gdn·HCl. To address this concern, we also performed duplicate runs using pairwise identical starting conformations equilibrated in Arg·HCl or Gdn·HCl solutions. For the pair highlighted in Figure 3J,K, the chains aggregated at $t = 81$ ns without additive, whereas with Arg·HCl they remained separated throughout the 150 ns window. Similarly, Figure 3L,M shows a pair of runs where aggregation without additive took place at $t = 39$ ns, while the chains did not aggregate in the presence of Gdn·HCl.

Robustness of MD-Predicted Aggregation Inhibition.

Multiple additional simulations were performed to verify the reproducibility of the trends shown in Figure 3. Figure S5 compiles data from eight triplicate runs starting with monomers equilibrated in water. Arg·HCl delayed or prevented aggregation in 7/8 of these runs, compared to the additive-free controls. Likewise, aggregation inhibition by Gdn·

HCl was seen in 7/8 runs. Pairwise runs for Arg·HCl-equilibrated chains resulted in 7/8 instances of aggregation delay or prevention by Arg·HCl (Figure S6). Finally, 8/8 pairwise runs starting from Gdn·HCl-equilibrated monomers showed aggregation delay or prevention by Gdn·HCl (Figure S7).

In summary, the MD simulations of Figures 3 and S5–S7 reproduce the experimental finding that both Arg·HCl and Gdn·HCl dramatically lower the aggregation propensity of Mb. This conclusion is based on a considerable number of MD data (56 runs in total with individual simulation windows up to $\sim 0.5\ \mu s$). Aggregation inhibition was observed regardless of the starting conditions, i.e., for monomers equilibrated in water, in Arg·HCl, or in Gdn·HCl. To the best of our knowledge, this is the first time that MD simulations directly captured the occurrence of aggregation inhibition by solvent additives.

Protein–Protein Contacts in Aggregated Dimers. An analysis of the MD data was performed to uncover the mechanism of aggregation inhibition by Arg·HCl and Gdn·HCl. As a first step, we examined the types of interactions in the aggregated dimers. We previously demonstrated⁸¹ that, in additive-free solutions, hydrophobic contacts involving L, I, V, F, and W play a major role for Mb aggregation. Also, K^+ residues participate in hydrophobic contacts through their butyl moieties (K^+ refers to lysine residues in single-letter code throughout this work, not potassium ions). In addition, aggregated chains were found to be linked by B^+/A^- salt bridges with $B = K$ or R , and $A = D$ or E .⁸¹ The existence of all these contacts was verified in the MD aggregates of the current work, both for additive-free solutions and in the presence of Arg·HCl or Gdn·HCl. Typical aggregated dimers are high-

lighted in Figure 4. Figure S8 provides a summary of all aggregates, illustrating the existence of salt bridges and hydrophobic interactions for all dimers generated here, even though the specific contact residues differed for individual MD runs. Overall, for those runs that produced an aggregate, there was no difference in the types of protein–protein contacts generated with and without additives. However, the formation propensity of these contacts was much lower in the presence of Arg-HCl or Gdn-HCl, evident from the fact that MD runs with these additives showed delayed or no aggregation.

Productive vs Unproductive Encounter Complexes.

When two protein chains aggregate, they must first form an encounter complex (defined as an arrangement where diffusive motions have brought the chains in close proximity to one another).¹¹¹ Some encounter complexes dissociate again after a few nanoseconds; i.e., not all of them culminate in firm protein–protein contacts. We will refer to these as “unproductive encounter complexes” (UECs). In contrast, “productive encounter complexes” (PECs) develop into firmly linked dimeric aggregates. Formation of PECs is indicated in the time profiles of Figures 3 (and S5–S7) with arrows, and we will now have a closer look at their structures. UECs will be discussed later.

Typical PECs are depicted in Figure 5 (Figure S8 shows the full data set). Regardless of the solvent conditions, almost all (35/37) PECs had hydrophobic protein–protein contacts. In contrast, the prevalence of intermolecular salt bridges in PECs was strongly affected by the presence of Arg-HCl or Gdn-HCl. Without additives, most (16/24) PECs had one or two salt bridges (Figures 5A and S8A–F). Only 13/32 runs in Arg-HCl or Gdn-HCl formed PECs. Strikingly, none of these 13 PECs had any salt bridges (Figures 5B,C, and S8G–K). We conclude that both Arg-HCl and Gdn-HCl suppress PEC formation by disfavoring protein–protein salt bridges. Because PECs are an obligatory step en route to aggregation, suppression of salt bridge formation will automatically lower the yield of aggregated proteins within a given time window. These conclusions are consistent with previous studies that noted the general importance of salt bridges and long-range electrostatics for biomolecular assembly processes.^{112,113}

Arg⁺ and Gdn⁺ Interactions with Mb. How exactly do Arg-HCl and Gdn-HCl suppress the formation of salt bridges? Figure 6A tracks interactions of Mb side chains and termini with Arg⁺ during a typical Arg-HCl run. Figure 6B normalizes these interactions by displaying fraction bound (f_b) values that account for the abundance of each moiety (e.g., Mb has 19 K⁺ but only 1 Ct⁻). D⁻ and E⁻ side chains as well as Ct⁻ were found to be Arg⁺ binding hotspots, with f_b values around 70% (Figure 6B). Less pronounced Arg⁺ binding was seen for Nt⁺ and K⁺, with f_b values of ~50% and ~40%, respectively. No other side chains exhibited a marked Arg⁺ binding affinity ($f_b < 30\%$). Figure 7A–D visualizes the nature of these binding interactions. The binding of Arg⁺ to D⁻/E⁻/Ct⁻ is mediated mostly by the Arg⁺ guanidinium group, which associates with protein carboxylates through ionic interactions and H-bonding (Figure 7A–C). Occasionally, the Arg⁺ amino group participates in carboxylate binding as well (Figure 7B). Binding of K⁺ involves charge–charge interactions and H-bonding with the Arg⁺ carboxylate (Figure 7D).

Binding contacts between Mb and Gdn⁺ resembled those for Arg⁺, with a strong preference for D⁻, E⁻, and Ct⁻ ($f_b > 0.9$, Figure 6C,D). Similar to Arg⁺, binding of Gdn⁺ to protein carboxylates was mediated by H-bond-reinforced ionic

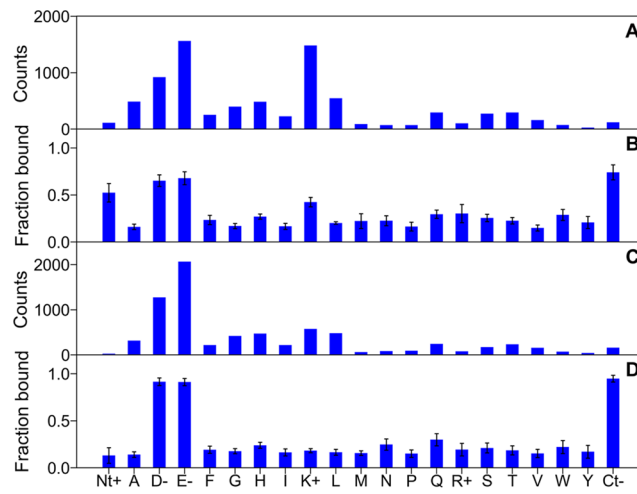


Figure 6. Contacts of Mb residues with Arg⁺ (A,B), and Gdn⁺ (C,D) prior to aggregation. Data were compiled by considering all protein atoms, as well as all Arg⁺ and Gdn⁺ atoms; a contact was defined as having a minimum protein-additive interatomic distance of $\leq 0.25 \text{ nm}$. Sampling was done in 5 ns intervals. Residues are listed along the bottom. (A) Unprocessed protein-Arg⁺ interaction counts for a typical trajectory. (B) Fraction bound, averaged for all Arg-HCl runs, and normalized to the abundance of different sites. Error bars represent standard deviations from all runs. (C,D) Same as in panels A and B, but for protein-Gdn⁺ interactions in Gdn-HCl-runs.

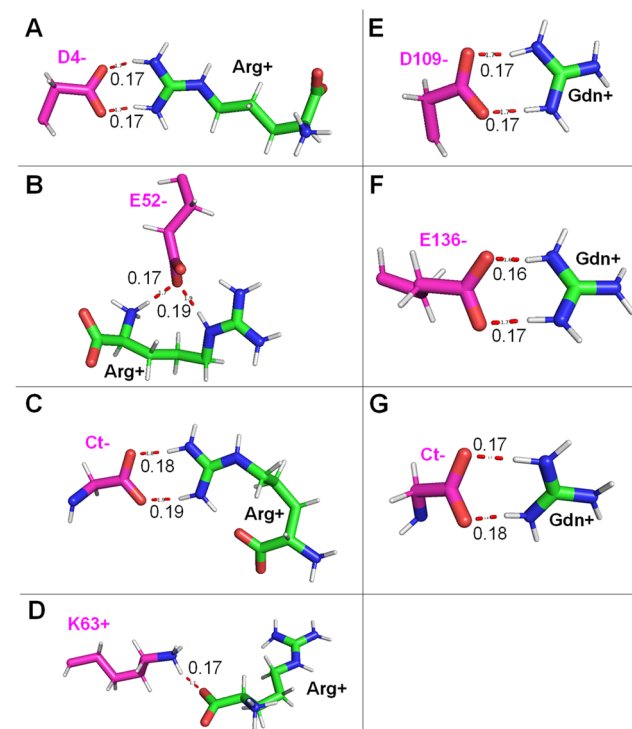


Figure 7. MD snapshots, illustrating preferred binding interactions between Mb and Arg⁺ (A–D) or Gdn⁺ (E–G). Protein residues are shown in magenta, Arg⁺ and Gdn⁺ are in green/blue, and oxygen is red. Dashed red lines represent H-bonds, with O...H distances indicated in nm.

interactions (Figure 7E–G). While Figure 7 highlights binding of Mb moieties to a single Arg⁺ (or Gdn⁺), there were also instances where multiple Arg⁺ (or Gdn⁺) interacted with one carboxylate (Figure S9).

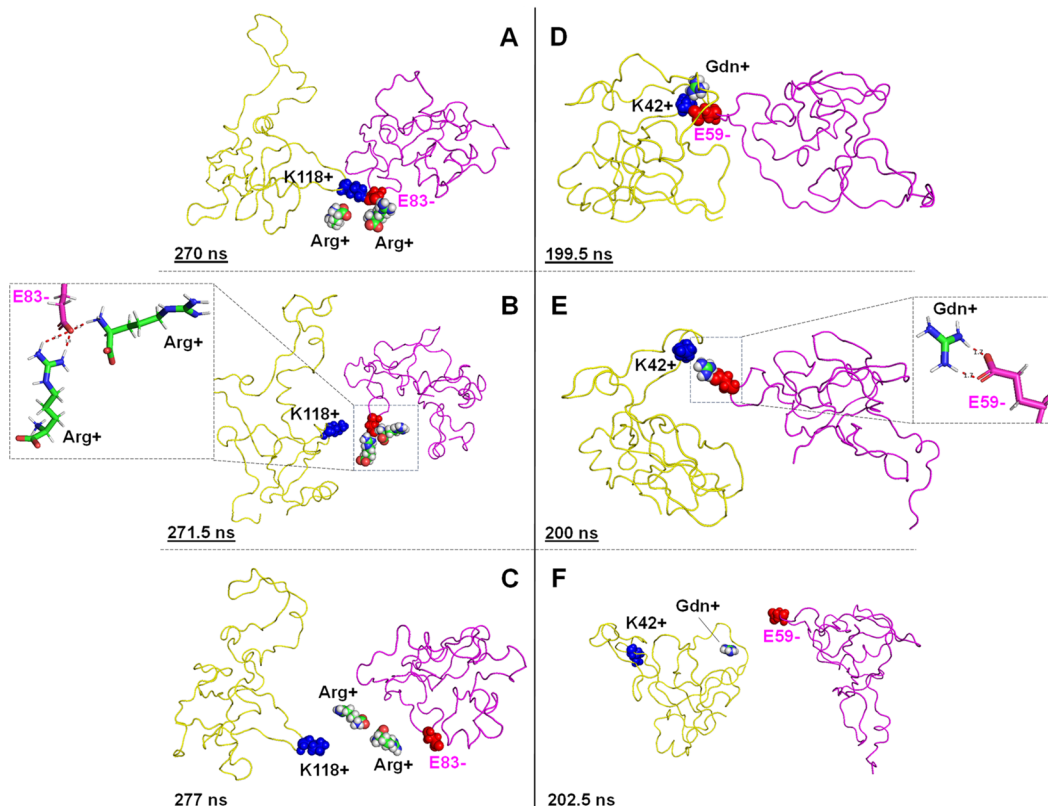


Figure 8. (A–C) Dissociation of an unproductive encounter complex (UEC) in the presence of Arg-HCl. The MD snapshots depict three closely spaced time points (Figure 3H asterisk). Panel B inset highlights E83[−] binding to two Arg⁺, after these two Arg⁺ dissociated the protein–protein salt bridge by outcompeting K118⁺. (D–F) Dissociation of a UEC in the presence of Gdn-HCl, covering the range marked with an asterisk in Figure 3I. Panel E inset highlights the Gdn⁺ that has outcompeted K42⁺ for salt bridge formation with E59[−].

In summary, our data show that Arg⁺ and Gdn⁺ interact with solvent-exposed side chains in a very similar fashion. Both additives primarily bind to protein carboxylates (D[−], E[−], and Ct[−]), by guanidinium-carboxylate ionic interactions and H-bonding. A slight difference between the two additives is that Arg⁺ also displays a certain affinity for amino groups (K⁺ and Nt⁺). In agreement with the data shown here, preferential Arg⁺ and Gdn⁺ binding to protein carboxylates has been noted in earlier studies.^{60,114} Other investigations proposed a much more promiscuous behavior, with Arg⁺ and Gdn⁺ binding to many additional protein moieties.^{54,59,61,80,115} Our data show that such other interactions are possible (including binding to aromatic residues) but with much lower specificity and affinity compared to the strong Arg⁺ and Gdn⁺ binding to carboxylates (Figures 6 and 7).

As discussed in more detail in the next section, binding of Arg⁺ and Gdn⁺ to D[−], E[−], and Ct[−] is the root cause of aggregation inhibition. These binding events lower the propensity of protein carboxylates to form intermolecular salt bridges with K⁺, R⁺, or Nt⁺. The highly abundant Arg⁺ and Gdn⁺ tend to outcompete K⁺, R⁺, or Nt⁺ during salt bridge formation. Inhibition of intramolecular salt bridges disfavors PEC formation, thereby lowering the number of aggregated proteins.

Unproductive Encounter Complexes. The mechanism by which Arg⁺ and Gdn⁺ affect the outcome of protein–protein encounters is directly evident from our MD trajectories. As noted, each encounter may give rise to a PEC that subsequently aggregates by maturation of weak initial contacts into firm hydrophobic and salt bridge linkages

(Figures 4 and 5). Alternatively, the encounter can result in a short-lived UEC that dissociates again. Figure 8A–C illustrates one of these UEC dissociation events, where two chains are initially in contact via a K⁺/E[−] salt bridge (Figure 8A). However, E[−] also interacts with two Arg⁺ ions, which then displace K⁺, thereby rupturing the salt bridge and allowing the proteins to separate from one another (Figure 8B,C). In a similar fashion, Figure 8D–F illustrates UEC dissociation triggered by Gdn⁺ that outcompetes K⁺ in a K⁺/E[−] salt bridge, causing the two proteins to separate instead of forming an aggregated dimer. In addition to illustrating how Arg⁺ and Gdn⁺ suppress protein–protein contacts, Figure 8 reveals that interactions of these additives with carboxylates are highly dynamic, as none of the additives remain associated with the protein for more than a few ns.

Self-Association of Arg⁺. Some earlier studies proposed that protein aggregation inhibition by Arg-HCl is mediated by [Arg⁺]_n clusters.^{55,60,63,80} Indeed, our MD simulations confirmed Arg⁺ self-association, reflecting the capability of Arg⁺ to form charge–charge contacts, and to act as both H-bond donor (with its guanidinium and amino groups) and H-bond acceptor (with its carboxylate).⁶⁰ However, we found no evidence of distinct [Arg⁺]_n clusters. Instead, all Arg⁺ formed an extended 3D network (Figure 9A,B). The ochre molecules in Figure 9B represent an arbitrarily selected subset of this quasi-infinite network that permeates the entire solution (green in Figure 9B). Thus, our data do not support the idea^{55,60,63,78} that distinct [Arg⁺]_n clusters are responsible for aggregation inhibition by Arg-HCl. In particular (as noted

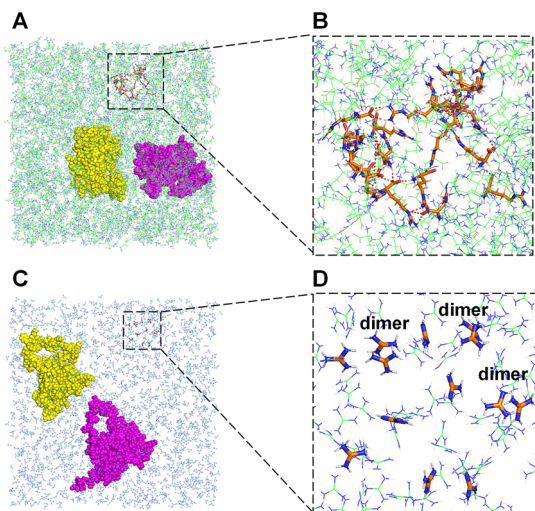


Figure 9. (A) Two Mb chains in 1 M Arg-HCl ($t = 300$ ns). For visualization, all solvent components except for Arg⁺ were omitted. (B) Closeup of the H-bonded Arg⁺ 3D network that extends through the entire solution. Only a small subset of this network is highlighted in ochre along with the corresponding H-bonds (red dashed lines). (C) Mb chains in 1 M Gdn-HCl. (D) Closeup of Gdn⁺ ions, most of which exist as monomers, while some form dimers.

previously⁶⁰), there is no MD evidence to support the idea of extended hydrophobic surfaces in such putative clusters.⁶³

The properties of Gdn⁺ in 1 M Gdn-HCl were visualized as well (Figure 9C,D). Most Gdn⁺ were found to exist as monomers, while a certain fraction formed [Gdn⁺]₂ species (noncovalent dimerization of Gdn⁺ has been reported previously).⁹⁶ The lack of a 3D H-bonded network for Gdn⁺ is unsurprising because Gdn⁺ does not possess any H-bond acceptors (unlike Arg⁺). The data presented in previous sections demonstrated that the mechanisms of protein aggregation inhibition by Arg⁺ and Gdn⁺ are very similar. The fact that only one of these additive (Arg⁺) undergoes self-association provides further evidence against the idea^{55,60,63,80} that [Arg⁺]_n clustering is an integral aspect of aggregation inhibition by Arg⁺.

CONCLUSIONS

Protein aggregation inhibition by Arg-HCl has profound practical implications, but the underlying principles have thus far remained enigmatic. The experiments and MD simulations of this work reveal a surprisingly simple mechanism. We found that aggregation inhibition by Arg-HCl is attributable to the guanidinium moiety of Arg⁺, which binds anionic side chains in a fashion similar to that of free Gdn⁺. In a nutshell, Arg⁺ inhibits aggregation by suppressing the formation of interprotein salt bridges, thereby reducing the “stickiness” of thermally unfolded proteins. Arg⁺ destabilizes the native state, i.e., it lowers T_m and thus pushes N ⇌ U equilibria of thermally stressed proteins toward the unfolded state. However, the magnitude of this destabilization is small enough to prevent unfolding in 1 M solution under ambient conditions, which is a key requirement for applications of Arg-HCl as an excipient in biopharmaceutical formulations.

In-depth analysis of our MD data revealed that Arg⁺ affects the fate of encounter complexes, i.e., short-lived species that are an obligatory step en route toward dimeric aggregation nuclei. Proteins in these encounter pairs are intermolecularly

linked by non-native hydrophobic contacts and salt bridges. Salt bridge formation is disfavored in the presence of Arg-HCl because Arg⁺ has a strong affinity for protein carboxylates (D⁻, E⁻, and Ct⁻) by forming H-bond-reinforced charge–charge contacts with these anionic sites. Arg⁺ binding dramatically lowers the D⁻, E⁻, and Ct⁻ propensity to form intermolecular salt bridges, because potential K⁺/R⁺ binding partners are outcompeted by Arg⁺. This reduced salt bridge formation propensity causes encounter complexes to dissociate instead of proceeding toward firmly linked mature aggregates. One can distinguish between productive and unproductive encounter complexes (PECs and UECs, respectively). By favoring UECs, Arg⁺ lowers the yield of aggregated protein.

The suppression of salt bridge formation seen in our work is not a trivial electrostatic screening effect.¹¹⁶ This is evident from the observation that 1 M Na⁺ does not suppress aggregation, whereas 1 M Arg⁺ is a highly effective aggregation inhibitor (Figure 2). Thus, the capability of Arg⁺ to interact with protein carboxylates both electrostatically and through H-bonds is an essential component of its aggregation inhibition mechanism (Figure 7).

While suppression of salt bridges by Arg⁺ and Gdn⁺ was identified as the main contributor to aggregation inhibition in this work, weakening of the hydrophobic effect (by alteration of the water structure) could be a contributing factor as well.^{117,118} However, this alternative aspect has previously shown to become significant only at much higher additive concentrations (e.g., [Gdn⁺] ≈ 5 M]),¹¹⁸ reinforcing the view that salt bridge destabilization is the dominant factor for aggregation inhibition under the conditions examined here.

Preferential interactions of Arg⁺ and Gdn⁺ with anionic protein sites have already been reported in some earlier MD studies, and it has even been proposed that such interaction could be involved in aggregation suppression.^{54,60,80} However, those earlier studies only examined inhibitor binding to monomeric proteins^{60,80} or preformed peptide oligomers.⁵⁴ Aggregate formation with and without additives was not compared, leaving the interpretation of those earlier data open to conjecture. In contrast, the simulations and experiments of the current work examined the association of monomeric proteins into aggregates, allowing us to deduce mechanistic details by comparing trajectories with and without inhibitors. To the best of our knowledge, such a direct MD-based demonstration of aggregation inhibition has never before been reported in the literature.

Given the chemical diversity of existing aggregation inhibitors,^{26,30,40–47} it cannot be expected that the mechanism uncovered here for Arg⁺ and Gdn⁺ equally applies to all other inhibitors. However, the blockage of protein–protein interaction sites by competitive binding is a common theme for some of them. For example, aggregation suppression by adenosine triphosphate (ATP) has been attributed, in part, to triphosphate interactions with K⁺ side chains.⁴⁷ Such ATP binding will interfere with the formation of interprotein salt bridges, analogously to the mechanism uncovered here where interprotein salt bridges are suppressed by Arg⁺ or Gdn⁺ binding to side chain carboxylates. Overall, it appears that MD simulations of the type performed here should be a general tool for uncovering aggregation inhibition mechanisms and for the *in silico* screening of newly designed inhibitors that have even greater efficacy than Arg⁺ and Gdn⁺.

ASSOCIATED CONTENT

SI Supporting Information

The Supporting Information is available free of charge at <https://pubs.acs.org/doi/10.1021/jacs.3c14180>.

Figure S1: production of thermally unfolded Mb starting structures for MD runs, Figure S2: thermal unfolding of Mb monitored by UV-vis and CD spectroscopy, Figure S3: time-dependent thermal aggregation experiments, Figure S4: Gdn-HCl-induced unfolding of Mb, Figure S5: triplicate sets of minimum distance vs time plots for Mb equilibrated in water, Figure S6: pairs of minimum distance vs time plots for Mb equilibrated in Arg-HCl, Figure S7: pairs of minimum distance vs time plots for Mb equilibrated in Gdn-HCl, Figure S8A–L: trajectory snapshots of productive encounter complexes and mature aggregates, and Figure S9: Arg and Gdn binding to Mb ([PDF](#))

Supporting movie of the Figure 3A–F MD data ([MP4](#))

AUTHOR INFORMATION

Corresponding Author

Lars Konermann — Department of Chemistry, The University of Western Ontario, London, Ontario N6A 5B7, Canada;
 orcid.org/0000-0002-5283-3165; Email: konerman@uwo.ca

Author

Yuen Ki Ng — Department of Chemistry, The University of Western Ontario, London, Ontario N6A 5B7, Canada;
 orcid.org/0000-0002-4818-2427

Complete contact information is available at:
<https://pubs.acs.org/10.1021/jacs.3c14180>

Notes

The authors declare no competing financial interest.

ACKNOWLEDGMENTS

Funding was provided by the Natural Sciences and Engineering Research Council of Canada (RGPIN-2018-04243). We thank Pablo Scrosati for help with the computational aspects of this work, as well as Lee-Ann Briere for help with CD experiments.

REFERENCES

- (1) Kazlauskas, R. Engineering more stable proteins. *Chem. Soc. Rev.* **2018**, *47* (24), 9026–9045.
- (2) Majid, N.; Khan, R. H. Protein aggregation: Consequences, mechanism, characterization and inhibitory strategies. *Int. J. Biol. Macromol.* **2023**, *242*, 125123.
- (3) Chiti, F.; Dobson, C. M. Protein Misfolding, Amyloid Formation, and Human Disease: A Summary of Progress Over the Last Decade. *Annu. Rev. Biochem.* **2017**, *86* (1), 27–68.
- (4) Hartl, F. U.; Hayer-Hartl, M. Converging concepts of protein folding *in vitro* and *in vivo*. *Nat. Struct. Mol. Biol.* **2009**, *16* (6), 574–581.
- (5) Cawood, E. E.; Karamanos, T. K.; Wilson, A. J.; Radford, S. E. Visualizing and trapping transient oligomers in amyloid assembly pathways. *Biophys. Chem.* **2021**, *268*, 106505.
- (6) Laganowsky, A.; Liu, C.; Sawaya, M. R.; Whitelegge, J. P.; Park, J.; Zhao, M.; Pensalfini, A.; Soriaga, A. B.; Landau, M.; Teng, P. K.; et al. Atomic view of a toxic amyloid small oligomer. *Science* **2012**, *335* (6073), 1228–1231.
- (7) Munneeruddin, K.; Thomas, J. J.; Salinas, P. A.; Kaltashov, I. A. Characterization of Small Protein Aggregates and Oligomers Using Size Exclusion Chromatography with Online Detection by Native Electrospray Ionization Mass Spectrometry. *Anal. Chem.* **2014**, *86* (21), 10692–10699.
- (8) Ye, S.; Hsiung, C.-H.; Tang, Y.; Zhang, X. Visualizing the Multistep Process of Protein Aggregation in Live Cells. *Acc. Chem. Res.* **2022**, *55* (3), 381–390.
- (9) Nguyen, P. H.; Ramamoorthy, A.; Sahoo, B. R.; Zheng, J.; Faller, P.; Straub, J. E.; Dominguez, L.; Shea, J.-E.; Dokholyan, N. V.; De Simone, A.; et al. Amyloid Oligomers: A Joint Experimental/Computational Perspective on Alzheimer’s Disease, Parkinson’s Disease, Type II Diabetes, and Amyotrophic Lateral Sclerosis. *Chem. Rev.* **2021**, *121* (4), 2545–2647.
- (10) Ahmed, R.; Melacini, G. A biophysical toolset to probe the microscopic processes underlying protein aggregation and its inhibition by molecular chaperones. *Biophys. Chem.* **2021**, *269*, 106508.
- (11) Vendruscolo, M. Proteome folding and aggregation. *Curr. Opin. Struct. Biol.* **2012**, *22* (2), 138–143.
- (12) Sekhar, A.; Rumfeldt, J. A. O.; Broom, H. R.; Doyle, C. M.; Bouvignies, G.; Meiering, E. M.; Kay, L. E. Thermal fluctuations of immature SOD1 lead to separate folding and misfolding pathways. *eLife* **2015**, *4*, No. e07296.
- (13) Zhu, S.; Shala, A.; Bezginov, A.; Sljoka, A.; Audette, G.; Wilson, D. J. Hyperphosphorylation of Intrinsically Disordered Tau Protein Induces an Amyloidogenic Shift in Its Conformational Ensemble. *PLoS One* **2015**, *10*, No. e0120416.
- (14) Seo, J.; Hoffmann, W.; Warnke, S.; Huang, X.; Gewinner, S.; Schollkopf, W.; Bowers, M. T.; von Helden, G.; Pagel, K. An infrared spectroscopy approach to follow β -sheet formation in peptide amyloid assemblies. *Nat. Chem.* **2017**, *9* (1), 39–44.
- (15) Stranks, S. D.; Ecroyd, H.; Van Sluyter, S.; Waters, E. J.; Carver, J. A.; von Smekal, L. Model for amorphous aggregation processes. *Phys. Rev. E* **2009**, *80* (5 Pt 1), 051907.
- (16) Borgia, M. B.; Nickson, A. A.; Clarke, J.; Hounslow, M. J. A Mechanistic Model for Amorphous Protein Aggregation of Immunoglobulin-like Domains. *J. Am. Chem. Soc.* **2013**, *135* (17), 6456–6464.
- (17) Bianco, V.; Alonso-Navarro, M.; Di Silvio, D.; Moya, S.; Cortajarena, A. L.; Coluzza, I. Proteins are Solitary! Pathways of Protein Folding and Aggregation in Protein Mixtures. *J. Phys. Chem. Lett.* **2019**, *10* (17), 4800–4804.
- (18) Greene, D. G.; Modla, S.; Wagner, N. J.; Sandler, S. I.; Lenhoff, A. M. Local Crystalline Structure in an Amorphous Protein Dense Phase. *Biophys. J.* **2015**, *109* (8), 1716–1723.
- (19) Penzkofer, A.; Shirdel, J.; Zirak, P.; Breitkreuz, H.; Wolf, E. Protein aggregation studied by forward light scattering and light transmission analysis. *Chem. Phys.* **2007**, *342* (1–3), 55–63.
- (20) Fink, A. L. Protein aggregation: folding aggregates, inclusion bodies and amyloid. *Folding Des.* **1998**, *3* (1), R9–R23.
- (21) Guzman, I.; Gruebele, M. Protein Folding Dynamics in the Cell. *J. Phys. Chem. B* **2014**, *118* (29), 8459–8470.
- (22) Hong, J.; Giersch, L. M. Macromolecular Crowding Remodels the Energy Landscape of a Protein by Favoring a More Compact Unfolded State. *J. Am. Chem. Soc.* **2010**, *132* (30), 10445–10452.
- (23) Buecheler, J. W.; Winzer, M.; Weber, C.; Gieseler, H. Oxidation-Induced Destabilization of Model Antibody-Drug Conjugates. *J. Pharm. Sci.* **2019**, *108* (3), 1236–1245.
- (24) Dong, A.; Randolph, T. W.; Carpenter, J. F. Entrapping Intermediates of Thermal Aggregation in α -Helical Proteins with Low Concentration of Guanidine Hydrochloride. *J. Biol. Chem.* **2000**, *275* (36), 27689–27693.
- (25) De Bernardez Clark, E.; Schwarz, E.; Rudolph, R. Inhibition of aggregation side reactions during *in vitro* protein folding. *Methods Enzymol.* **1999**, *309*, 217–236.
- (26) Singh, A.; Upadhyay, V.; Upadhyay, A. K.; Singh, S. M.; Panda, A. K. Protein recovery from inclusion bodies of *Escherichia coli* using mild solubilization process. *Microb. Cell Fact.* **2015**, *14*, 41.

- (27) Golovanov, A. P.; Hautbergue, G. M.; Wilson, S. A.; Lian, L. Y. A simple method for improving protein solubility and long-term stability. *J. Am. Chem. Soc.* **2004**, *126* (29), 8933–8939.
- (28) Roberts, C. J.; Das, T. K.; Sahin, E. Predicting solution aggregation rates for therapeutic proteins: Approaches and challenges. *Int. J. Pharm.* **2011**, *418* (2), 318–333.
- (29) Heads, J. T.; Kelm, S.; Tyson, K.; Lawson, A. D. G. A computational method for predicting the aggregation propensity of IgG1 and IgG4(P) mAbs in common storage buffers. *mAbs* **2022**, *14* (1), 2138092.
- (30) Roberts, C. J. Protein aggregation and its impact on product quality. *Curr. Opin. Biotechnol.* **2014**, *30*, 211–217.
- (31) Moussa, E. M.; Panchal, J. P.; Moorthy, B. S.; Blum, J. S.; Joubert, M. K.; Narhi, L. O.; Topp, E. M. Immunogenicity of Therapeutic Protein Aggregates. *J. Pharm. Sci.* **2016**, *105* (2), 417–430.
- (32) Young, L. M.; Saunders, J. C.; Mahood, R. A.; Revill, C. H.; Foster, R. J.; Tu, L.-H.; Raleigh, D. P.; Radford, S. E.; Ashcroft, A. E. Screening and classifying small-molecule inhibitors of amyloid formation using ion mobility spectrometry–mass spectrometry. *Nat. Chem.* **2015**, *7* (1), 73–81.
- (33) Sanders, H. M.; Jovcevski, B.; Marty, M. T.; Pukala, T. L. Structural and mechanistic insights into amyloid- β and α -synuclein fibril formation and polyphenol inhibitor efficacy in phospholipid bilayers. *FEBS J.* **2022**, *289* (1), 215–230.
- (34) Hopper, J. T. S.; Robinson, C. V. Mass Spectrometry Quantifies Protein Interactions—From Molecular Chaperones to Membrane Porins. *Angew. Chem., Int. Ed.* **2014**, *53* (51), 14002–14015.
- (35) Balchin, D.; Hayer-Hartl, M.; Hartl, F. U. In vivo aspects of protein folding and quality control. *Science* **2016**, *353* (6294), 42.
- (36) Schmidpeter, P. A. M.; Schmid, F. X. Prolyl Isomerization and Its Catalysis in Protein Folding and Protein Function. *J. Mol. Biol.* **2015**, *427* (7), 1609–1631.
- (37) Saibil, H. Chaperone machines for protein folding, unfolding and disaggregation. *Nat. Rev. Mol. Cell Biol.* **2013**, *14* (10), 630–642.
- (38) Shtrimerman, M.; Lorimer, G. H.; Englander, S. W. Chaperonin Function: Folding by Forced Unfolding. *Science* **1999**, *284* (5415), 822–825.
- (39) Karamanos, T. K.; Clore, G. M. Large Chaperone Complexes Through the Lens of Nuclear Magnetic Resonance Spectroscopy. *Annu. Rev. Biophys.* **2022**, *51* (1), 223–246.
- (40) Gault, J.; Lianoudaki, D.; Kaldmae, M.; Kronqvist, N.; Rising, A.; Johansson, J.; Lohkamp, B.; Lain, S.; Allison, T. M.; Lane, D. P.; et al. Mass Spectrometry Reveals the Direct Action of a Chemical Chaperone. *J. Phys. Chem. Lett.* **2018**, *9* (14), 4082–4086.
- (41) Sharma, S.; Sarkar, S.; Paul, S. S.; Roy, S.; Chattopadhyay, K. A small molecule chemical chaperone optimizes its unfolded state contraction and denaturant like properties. *Sci. Rep.* **2013**, *3*, 3525.
- (42) Wu, X.; Deng, F.; Chen, Y.; Xu, M.; Ma, F.; Shi, L. Electrostatic and hydrophobic interaction cooperative nanochaperone regulates protein folding. *Aggregate* **2024**, *5* (1), No. e429.
- (43) Cortez, L.; Sim, V. The therapeutic potential of chemical chaperones in protein folding diseases. *Prion* **2014**, *8* (2), 197–202.
- (44) Park, I. S.; Kim, S.; Yim, Y.; Park, G.; Choi, J.; Won, C.; Min, D. H. Multifunctional synthetic nano-chaperone for peptide folding and intracellular delivery. *Nat. Commun.* **2022**, *13* (1), 4568.
- (45) Ignatova, Z.; Giersch, L. M. Inhibition of protein aggregation in vitro and in vivo by a natural osmoprotectant. *Proc. Natl. Acad. Sci. U. S. A.* **2006**, *103* (36), 13357–13361.
- (46) Patel, A.; Malinovska, L.; Saha, S.; Wang, J.; Alberti, S.; Krishnan, Y.; Hyman, A. A. ATP as a biological hydrotrope. *Science* **2017**, *356* (6339), 753–756.
- (47) Mehringer, J.; Do, T. M.; Touraud, D.; Hohenschutz, M.; Khoshshima, A.; Horinek, D.; Kunz, W. Hofmeister versus Neuberg: is ATP really a biological hydrotrope? *Cell Rep. Phys. Sci.* **2021**, *2* (2), 100343.
- (48) Bye, J. W.; Platts, L.; Falconer, R. J. Biopharmaceutical liquid formulation: a review of the science of protein stability and solubility in aqueous environments. *Biotechnol. Lett.* **2014**, *36* (5), 869–875.
- (49) Toth, R. T.; Pace, S. E.; Mills, B. J.; Joshi, S. B.; Esfandiary, R.; Middaugh, C. R.; Weis, D. D.; Volkin, D. B. Evaluation of Hydrogen Exchange Mass Spectrometry as a Stability-Indicating Method for Formulation Excipient Screening for an IgG4Monoclonal Antibody. *J. Pharm. Sci.* **2018**, *107* (4), 1009–1019.
- (50) Goldberg, D. S.; Lewus, R. A.; Esfandiary, R.; Farkas, D. C.; Mody, N.; Day, K. J.; Mallik, P.; Tracka, M. B.; Sealey, S. K.; Samra, H. S. Utility of High Throughput Screening Techniques to Predict Stability of Monoclonal Antibody Formulations During Early Stage Development. *J. Pharm. Sci.* **2017**, *106* (8), 1971–1977.
- (51) Kamerzell, T. J.; Esfandiary, R.; Joshi, S. B.; Middaugh, C. R.; Volkin, D. B. Protein–excipient interactions: Mechanisms and biophysical characterization applied to protein formulation development. *Adv. Drug Deliv. Rev.* **2011**, *63* (13), 1118–1159.
- (52) Jo, S.; Xu, A.; Curtis, J. E.; Somani, S.; MacKrell, A. D., Jr. Computational Characterization of Antibody–Excipient Interactions for Rational Excipient Selection Using the Site Identification by Ligand Competitive Saturation-Biologics Approach. *Mol. Pharmaceutics* **2020**, *17* (11), 4323–4333.
- (53) Oki, S.; Nishinami, S.; Nakuchi, Y.; Ogura, T.; Shiraki, K. Arginine and its Derivatives Suppress the Opalescence of an Antibody Solution. *J. Pharm. Sci.* **2022**, *111* (4), 1126–1132.
- (54) Březina, K.; Duboué-Dijon, E.; Palivec, V.; Jiráček, J.; Kržík, T.; Viola, C. M.; Ganderton, T. R.; Brzozowski, A. M.; Jungwirth, P. Can Arginine Inhibit Insulin Aggregation? A Combined Protein Crystallography, Capillary Electrophoresis, and Molecular Simulation Study. *J. Phys. Chem. B* **2018**, *122* (44), 10069–10076.
- (55) Mamsa, S. S. A.; Meloni, B. P. Arginine and Arginine-Rich Peptides as Modulators of Protein Aggregation and Cytotoxicity Associated With Alzheimer’s Disease. *Front. Mol. Neurosci.* **2021**, *14*, 759729.
- (56) Shiraki, K.; Kudou, M.; Fujiwara, S.; Imanaka, T.; Takagi, M. Biophysical effect of amino acids on the prevention of protein aggregation. *J. Biochem.* **2002**, *132* (4), 591–595.
- (57) Fersht, A. R. *Structure and Mechanism in Protein Science*; W. H. Freeman & Co.: New York, 1999.
- (58) Rudolph, R.; Fischer, S.; Mattes, R. Process for the activating of gene-technologically produced, heterologous, disulphide bridge-containing eukaryotic proteins after expression in prokaryotes. United States Patent US 5,593,865 A, 1997, 1–20
- (59) Tsumoto, K.; Umetsu, M.; Kumagai, I.; Ejima, D.; Philo, J. S.; Arakawa, T. Role of arginine in protein refolding, solubilization, and purification. *Biotechnol. Prog.* **2004**, *20* (5), 1301–1308.
- (60) Shukla, D.; Trout, B. L. Interaction of Arginine with Proteins and the Mechanism by Which It Inhibits Aggregation. *J. Phys. Chem. B* **2010**, *114* (42), 13426–13438.
- (61) Arakawa, T.; Ejima, D.; Tsumoto, K.; Obeyama, N.; Tanaka, Y.; Kita, Y.; Timasheff, S. N. Suppression of protein interactions by arginine: A proposed mechanism of the arginine effects. *Biophys. Chem.* **2007**, *127* (1–2), 1–8.
- (62) Platts, L.; Falconer, R. J. Controlling protein stability: Mechanisms revealed using formulations of arginine, glycine and guanidinium HCl with three globular proteins. *Int. J. Pharm.* **2015**, *486* (1–2), 131–135.
- (63) Das, U.; Hariprasad, G.; Ethayathulla, A. S.; Manral, P.; Das, T. K.; Pasha, S.; Mann, A.; Ganguli, M.; Verma, A. K.; Bhat, R.; et al. Inhibition of Protein Aggregation: Supramolecular Assemblies of Arginine Hold the Key. *PLoS One* **2007**, *2* (11), No. e1176.
- (64) Shukla, D.; Trout, B. L. Preferential Interaction Coefficients of Proteins in Aqueous Arginine Solutions and Their Molecular Origins. *J. Phys. Chem. B* **2011**, *115* (5), 1243–1253.
- (65) Lyutova, E. M.; Kasakov, A. S.; Gurvits, B. Y. Effects of arginine on kinetics of protein aggregation studied by dynamic laser light scattering and turbidimetry techniques. *Biotechnol. Prog.* **2007**, *23* (6), 1411–1416.
- (66) Hirano, A.; Kameda, T.; Shinohara, D.; Arakawa, T.; Shiraki, K. Molecular Dynamics Simulation of the Arginine-Assisted Solubilization of Caffeic Acid: Intervention in the Interaction. *J. Phys. Chem. B* **2013**, *117* (25), 7518–7527.

- (67) Santra, S.; Jana, M. Influence of Aqueous Arginine Solution on Regulating Conformational Stability and Hydration Properties of the Secondary Structural Segments of a Protein at Elevated Temperatures: A Molecular Dynamics Study. *J. Phys. Chem. B* **2022**, *126* (7), 1462–1476.
- (68) Shukla, D.; Schneider, C. P.; Trout, B. L. Complex Interactions between Molecular Ions in Solution and Their Effect on Protein Stability. *J. Am. Chem. Soc.* **2011**, *133* (46), 18713–18718.
- (69) Wang, L.; Zhang, Y.; Li, R.; Xiang, D. L-lysine moderates thermal aggregation of coconut proteins induced by thermal treatment. *Sci. Rep.* **2023**, *13* (1), 13310.
- (70) Piana, S.; Lindorff-Larsen, K.; Shaw, D. E. Atomic-level description of ubiquitin folding. *Proc. Natl. Acad. Sci. U. S. A.* **2013**, *110* (15), 5915–5920.
- (71) Voelz, V. A.; Pande, V. S.; Bowman, G. R. Folding@home: Achievements from over 20 years of citizen science herald the exascale era. *Biophys. J.* **2023**, *122* (14), 2852–2863.
- (72) Adhikari, U.; Mostofian, B.; Copperman, J.; Subramanian, S. R.; Petersen, A. A.; Zuckerman, D. M. Computational Estimation of Microsecond to Second Atomistic Folding Times. *J. Am. Chem. Soc.* **2019**, *141* (16), 6519–6526.
- (73) Abraham, M. J.; Murtola, T.; Schulz, R.; Páll, S.; Smith, J. C.; Hess, B.; Lindahl, E. GROMACS: High performance molecular simulations through multi-level parallelism from laptops to supercomputers. *SoftwareX* **2015**, *1*, 19–25.
- (74) Barz, B.; Liao, Q.; Strodel, B. Pathways of Amyloid- β Aggregation Depend on Oligomer Shape. *J. Am. Chem. Soc.* **2018**, *140* (1), 319–327.
- (75) Ilie, I. M.; Caflisch, A. Simulation Studies of Amyloidogenic Polypeptides and Their Aggregates. *Chem. Rev.* **2019**, *119* (12), 6956–6993.
- (76) Lemkul, J. A.; Bevan, D. R. Assessing the Stability of Alzheimer's Amyloid Protofibrils Using Molecular Dynamics. *J. Phys. Chem. B* **2010**, *114* (4), 1652–1660.
- (77) Wu, M.; Dorosh, L.; Schmitt-Ulms, G.; Wille, H.; Stepanova, M. Aggregation of $\text{A}\beta$ 40/42 chains in the presence of cyclic neuropeptides investigated by molecular dynamics simulations. *PLoS Comput. Biol.* **2021**, *17* (3), No. e1008771.
- (78) Paul, R.; Bera, S.; Devi, M.; Paul, S. S. Inhibition of $\text{A}\beta_{16-22}$ Peptide Aggregation by Small Molecules and Their Permeation through POPC Lipid Bilayer: Insight from Molecular Dynamics Simulation Study. *J. Chem. Inf. Model.* **2022**, *62* (21), 5193–5207.
- (79) Lao, Z.; Chen, Y.; Tang, Y.; Wei, G. Molecular Dynamics Simulations Reveal the Inhibitory Mechanism of Dopamine against Human Islet Amyloid Polypeptide (hIAPP) Aggregation and Its Destabilization Effect on hIAPP Protofibrils. *ACS Chem. Neurosci.* **2019**, *10* (9), 4151–4159.
- (80) Vagenende, V.; Han, A. X.; Mueller, M.; Trout, B. L. Protein-Associated Cation Clusters in Aqueous Arginine Solutions and Their Effects on Protein Stability and Size. *ACS Chem. Biol.* **2013**, *8* (2), 416–422.
- (81) Ng, Y. K.; Tajuddin, N. N.; Scrosati, P. M.; Konermann, L. Mechanism of Thermal Protein Aggregation: Experiments and Molecular Dynamics Simulations on the High-Temperature Behavior of Myoglobin. *J. Phys. Chem. B* **2021**, *125* (48), 13099–13110.
- (82) Eliezer, D.; Yao, J.; Dyson, H. J.; Wright, P. E. Structural and dynamic characterization of partially folded states of apomyoglobin and implications for protein folding. *Nat. Struct. Biol.* **1998**, *5* (2), 148–155.
- (83) Privalov, P. L.; Griko, Y. V.; Venyaminov, S. Y.; Kutyshenko, V. P. Cold Denaturation of Myoglobin. *J. Mol. Biol.* **1986**, *190* (3), 487–498.
- (84) Frauenfelder, H.; Chen, G.; Berendzen, J.; Fenimore, P. W.; Jansson, H.; McMahon, B. H.; Stroe, I. R.; Swenson, J.; Young, R. D. A unified model of protein dynamics. *Proc. Natl. Acad. Sci. U. S. A.* **2009**, *106* (13), 5129–5134.
- (85) Fändrich, M.; Fletcher, M. A.; Dobson, C. M. Amyloid fibrils from muscle myoglobin. *Nature* **2001**, *410* (6825), 165–166.
- (86) Meersman, F.; Smeller, L.; Heremans, K. Comparative Fourier transform infrared spectroscopy study of cold-, pressure-, and heat-induced unfolding and aggregation of myoglobin. *Biophys. J.* **2002**, *82* (5), 2635–2644.
- (87) Yang, M.; Dutta, C.; Tiwari, A. Disulfide-Bond Scrambling Promotes Amorphous Aggregates in Lysozyme and Bovine Serum Albumin. *J. Phys. Chem. B* **2015**, *119* (10), 3969–3981.
- (88) Futami, J.; Miyamoto, A.; Hagimoto, A.; Suzuki, S.; Futami, M.; Tada, H. Evaluation of irreversible protein thermal inactivation caused by breakage of disulphide bonds using methanethiosulphonate. *Sci. Rep.* **2017**, *7* (1), 12471.
- (89) Swint, L.; Robertson, A. D. Thermodynamics of unfolding for turkey ovomucoid third domain: Thermal and chemical denaturation. *Protein Sci.* **1993**, *2* (12), 2037–2049.
- (90) Huang, J.; Rauscher, S.; Nawrocki, G.; Ran, T.; Feig, M.; de Groot, B. L.; Grubmuller, H.; MacKerell, A. D. CHARMM36m: an improved force field for folded and intrinsically disordered proteins. *Nat. Methods* **2017**, *14* (1), 71–73.
- (91) Jorgensen, W. L.; Chandrasekhar, J.; Madura, J. D.; Impey, R. W.; Klein, M. L. Comparison of simple potential functions for simulating liquid water. *J. Chem. Phys.* **1983**, *79* (2), 926–935.
- (92) Krammer, E.-M.; Ghaddar, K.; André, B.; Prévost, M. Unveiling the Mechanism of Arginine Transport through AdiC with Molecular Dynamics Simulations: The Guiding Role of Aromatic Residues. *PLoS One* **2016**, *11* (8), No. e0160219.
- (93) Lee, J.; Cheng, X.; Swails, J. M.; Yeom, M. S.; Eastman, P. K.; Lemkul, J. A.; Wei, S.; Buckner, J.; Jeong, J. C.; Qi, Y.; et al. CHARMM-GUI Input Generator for NAMD, GROMACS, AMBER, OpenMM, and CHARMM/OpenMM Simulations Using the CHARMM36 Additive Force Field. *J. Chem. Theory Comput.* **2016**, *12* (1), 405–413.
- (94) Javanshad, R.; Venter, A. R. Effects of amino acid additives on protein solubility – insights from desorption and direct electrospray ionization mass spectrometry. *Analyst* **2021**, *146* (21), 6592–6604.
- (95) Lange, C.; Rudolph, R. Suppression of Protein Aggregation by L-Arginine. *Curr. Pharm. Biotechnol.* **2009**, *10* (4), 408–414.
- (96) Vazdar, M.; Heyda, J.; Mason, P. E.; Tesei, G.; Allolio, C.; Lund, M.; Jungwirth, P. Arginine “Magic”: Guanidinium Like-Charge Ion Pairing from Aqueous Salts to Cell Penetrating Peptides. *Acc. Chem. Res.* **2018**, *51* (6), 1455–1464.
- (97) Konermann, L.; Rosell, F. I.; Mauk, A. G.; Douglas, D. J. Acid-Induced Denaturation of Myoglobin Studied by Time-Resolved Electrospray Ionization Mass Spectrometry. *Biochemistry* **1997**, *36* (21), 6448–6454.
- (98) Pace, C. N.; Vajdos, F.; Fee, L.; Grimsley, G.; Gray, T. How to measure and predict the molar absorption coefficient of a protein. *Protein Sci.* **1995**, *4* (11), 2411–2423.
- (99) Menzen, T.; Friess, W. High-throughput melting-temperature analysis of a monoclonal antibody by differential scanning fluorimetry in the presence of surfactants. *J. Pharm. Sci.* **2013**, *102* (2), 415–428.
- (100) Arthur, K. K.; Dinh, N.; Gabrielson, J. P. Technical Decision Making with Higher Order Structure Data: Utilization of Differential Scanning Calorimetry to Elucidate Critical Protein Structural Changes Resulting from Oxidation. *J. Pharm. Sci.* **2015**, *104* (4), 1548–1554.
- (101) Longo, L. M.; Gao, Y.; Tenorio, C. A.; Wang, G.; Paravastu, A. K.; Blaber, M. Folding nucleus structure persists in thermally-aggregated FGF-1. *Protein Sci.* **2018**, *27* (2), 431–440.
- (102) Shivu, B.; Seshadri, S.; Li, J.; Oberg, K. A.; Uversky, V. N.; Fink, A. L. Distinct β -Sheet Structure in Protein Aggregates Determined by ATR-FTIR Spectroscopy. *Biochemistry* **2013**, *52* (31), 5176–5183.
- (103) Horvath, G.; Biczok, L.; Majer, Z.; Kovacs, M.; Micsonai, A.; Kardos, J.; Toke, O. Structural insight into a partially unfolded state preceding aggregation in an intracellular lipid-binding protein. *FEBS J.* **2017**, *284* (21), 3637–3661.
- (104) Mashaghi, A.; Bezrukavnikov, S.; Minde, D. P.; Wentink, A. S.; Kityk, R.; Zachmann-Brand, B.; Mayer, M. P.; Kramer, G.; Bukau, B.; Tans, S. J. Alternative modes of client binding enable functional plasticity of Hsp70. *Nature* **2016**, *539* (7629), 448–451.

- (105) Hingorani, K. S.; Metcalf, M. C.; Deming, D. T.; Garman, S. C.; Powers, E. T.; Giersch, L. M. Ligand-promoted protein folding by biased kinetic partitioning. *Nat. Chem. Biol.* **2017**, *13* (4), 369–371.
- (106) Wang, G.; Abzalimov, R. R.; Kaltashov, I. A. Direct Monitoring of Heat-Stressed Biopolymers with Temperature-Controlled Electrospray Ionization Mass Spectrometry. *Anal. Chem.* **2011**, *83* (8), 2870–2876.
- (107) Ishibashi, M.; Tsumoto, K.; Tokunaga, M.; Ejima, D.; Kita, Y.; Arakawa, T. Is arginine a protein-denaturant? *Protein Expression Purif.* **2005**, *42* (1), 1–6.
- (108) Kim, N. A.; Hada, S.; Thapa, R.; Jeong, S. H. Arginine as a protein stabilizer and destabilizer in liquid formulations. *Int. J. Pharm.* **2016**, *513* (1–2), 26–37.
- (109) Liu, F.; Gruebele, M. Mapping an Aggregation Nucleus One Protein at a Time. *J. Phys. Chem. Lett.* **2010**, *1* (1), 16–19.
- (110) Zhang, Y.; Rempel, D. L.; Zhang, J.; Sharma, A. K.; Mirica, L. M.; Gross, M. L. Pulsed hydrogen–deuterium exchange mass spectrometry probes conformational changes in amyloid beta ($A\beta$) peptide aggregation. *Proc. Natl. Acad. Sci. U. S. A.* **2013**, *110* (36), 14604–14609.
- (111) Kozakov, D.; Li, K. Y.; Hall, D. R.; Beglov, D.; Zheng, J. F.; Vakili, P.; Schueler-Furman, O.; Paschalidis, I. C.; Clore, G. M.; Vajda, S. Encounter complexes and dimensionality reduction in protein–protein association. *eLife* **2014**, *3*, No. e01370.
- (112) Di Savino, A.; Foerster, J. M.; La Haye, T.; Blok, A.; Timmer, M.; Ullmann, G. M.; Ubbink, M. Efficient Encounter Complex Formation and Electron Transfer to Cytochrome c Peroxidase with an Additional, Distant Electrostatic Binding Site. *Angew. Chem., Int. Ed.* **2020**, *59* (51), 23239–23243.
- (113) Ivanov, D. G.; Ivetic, N.; Du, Y.; Nguyen, S. N.; Le, S. H.; Favre, D.; Nazy, I.; Kaltashov, I. A. Reverse Engineering of a Pathogenic Antibody Reveals the Molecular Mechanism of Vaccine-Induced Immune Thrombotic Thrombocytopenia. *J. Am. Chem. Soc.* **2023**, *145* (46), 25203–25213.
- (114) Chan, A. W. E.; Laskowski, R. A.; Selwood, D. L. Chemical Fragments that Hydrogen Bond to Asp, Glu, Arg, and His Side Chains in Protein Binding Sites. *J. Med. Chem.* **2010**, *53* (8), 3086–3094.
- (115) Mason, P. E.; Brady, J. W.; Neilson, G. W.; Dempsey, C. E. The interaction of guanidinium ions with a model peptide. *Biophys. J.* **2007**, *93* (1), L04–L06.
- (116) Kumar, S.; Nussinov, R. Salt bridge stability in monomeric proteins. *J. Mol. Biol.* **1999**, *293* (5), 1241–1255.
- (117) Lim, W. K.; Rosgen, J.; Englander, S. W. Urea, but not guanidinium, destabilizes proteins by forming hydrogen bonds to the peptide group. *Proc. Natl. Acad. Sci. U. S. A.* **2009**, *106* (8), 2595–2600.
- (118) England, J. L.; Pande, V. S.; Haran, G. Chemical Denaturants Inhibit the Onset of Dewetting. *J. Am. Chem. Soc.* **2008**, *130* (36), 11854–11855.